

Silicon nanowire network metal-semiconductor-metal photodetectors

Emre Mulazimoglu, Sahin Coskun, Mete Gunoven, Bayram Butun, Ekmel Ozbay et al.

Citation: *Appl. Phys. Lett.* **103**, 083114 (2013); doi: 10.1063/1.4819387

View online: <http://dx.doi.org/10.1063/1.4819387>

View Table of Contents: <http://apl.aip.org/resource/1/APPLAB/v103/i8>

Published by the [AIP Publishing LLC](#).

Additional information on *Appl. Phys. Lett.*

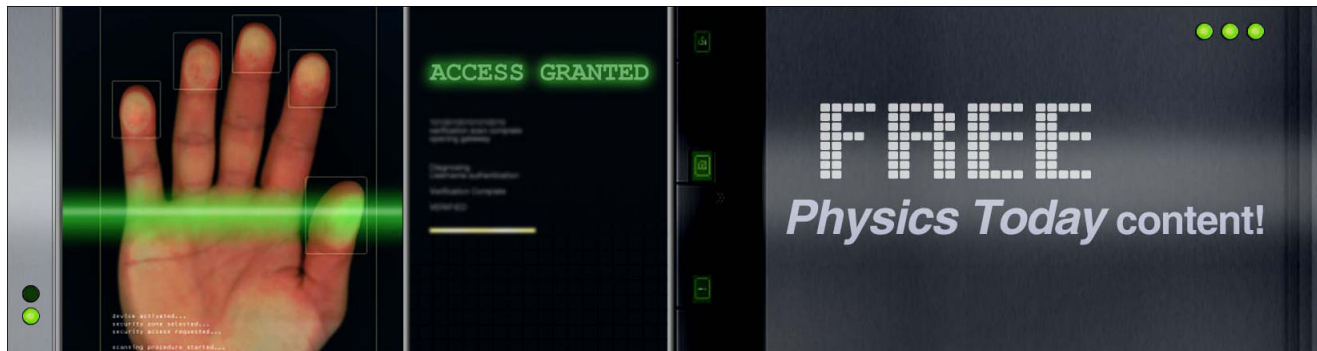
Journal Homepage: <http://apl.aip.org/>

Journal Information: http://apl.aip.org/about/about_the_journal

Top downloads: http://apl.aip.org/features/most_downloaded

Information for Authors: <http://apl.aip.org/authors>

ADVERTISEMENT



Silicon nanowire network metal-semiconductor-metal photodetectors

Emre Mulazimoglu,^{1,2} Sahin Coskun,¹ Mete Gunoven,^{2,3} Bayram Butun,⁴ Ekmel Ozbay,^{4,5} Rasit Turan,^{2,3} and Husnu Emrah Unalan^{1,2,a)}

¹Department of Metallurgical and Materials Engineering, Middle East Technical University, Ankara 06800, Turkey

²Center for Solar Energy Research and Applications (GÜNAM), Middle East Technical University, Ankara 06800, Turkey

³Department of Physics, Middle East Technical University, Ankara 06800, Turkey

⁴Nanotechnology Research Center, Bilkent University, Ankara 06800, Turkey

⁵Department of Electrical and Electronics Engineering, Department of Physics, Bilkent University, Ankara 06800, Turkey

(Received 1 June 2013; accepted 11 August 2013; published online 23 August 2013)

We report on the fabrication and characterization of solution-processed, highly flexible, silicon nanowire network based metal-semiconductor-metal photodetectors. Both the active part of the device and the electrodes are made of nanowire networks that provide both flexibility and transparency. Fabricated photodetectors showed a fast dynamic response, 0.43 ms for the rise and 0.58 ms for the fall-time, with a decent on/off ratio of 20. The effect of nanowire-density on transmittance and light on/off behavior were both investigated. Flexible photodetectors, on the other hand, were fabricated on polyethyleneterephthalate substrates and showed similar photodetector characteristics upon bending down to a radius of 1 cm. © 2013 AIP Publishing LLC.

[<http://dx.doi.org/10.1063/1.4819387>]

With the recent developments of nanomaterials and nanotechnology, one dimensional (1D) materials have received intense attention due to new functionalities such as quantum confinement and efficient charge transport.¹ Being the major material of the semiconductor industry, silicon nanowires (Si NWs) have become one of the most emergent 1D materials. With the well-tailored electrical and optical properties and high degree of excellence in the material and device processing, Si offers a superior performance also in reduced dimensions. Up to now, different fabrication routes have been reported for Si NWs. As the bottom-up approaches vapor-liquid-solid (VLS),² molecular beam epitaxy (MBE),³ supercritical fluid liquid solid (SFLS),⁴ and laser ablation⁵ have been utilized. Alternatively, top-down approaches including lithographical methods,⁶ deep reactive ion etching (DRIE)⁷ and, most recently, the facile metal-assisted-chemical etching (MAE) method^{8–18} have been introduced.

Bottom-up methods usually necessitate complex equipment, high temperatures, vacuum, and hazardous Si precursors, all of which drastically increase the cost of the processes. However, top-down approaches and especially the MAE method allow for cost effective fabrication. It is a powerful, simple, and solution-based process. It allows the fabrication of Si NW arrays over large areas without patterning prior to the etching process. We have recently demonstrated their applications on large area, industrial sized solar cells.¹⁹ By the nature of the process, the resulting Si NWs inherit the starting wafer characteristics, such as the doping type, density, conductivity, and crystal orientation.¹

Si NWs have been used in a wide range of prototype applications, such as solar cells,^{19–28} field effect transistors (FETs),^{29,30} thermoelectric applications,^{31,32} lithium batteries,^{33,34} light emitting diodes (LEDs),³⁵ and photodetectors.^{36–43}

The research activities on photodetector technology have been focused on obtaining miniaturized devices with high responsivity, large bandwidth, short response time, low noise, and high gain. Some of these performance properties could be achieved in devices with thick active layers. On the other hand, in some applications, thin active layers are required to reduce the carrier transit time for short response times. Moreover, they offer flexibility and partial transparency.

The use of Si NWs in photodetectors has already been demonstrated in two different forms. The first one utilizes the vertical arrays of Si NWs as the active layer of the device.^{36,41,44} Although this morphology gives enhanced light harvesting and high quantum efficiencies, the rigidity of the structure prevents flexible applications. In the second form, planar single/multiple Si NW(s) have been used as the active layer of the devices. This form is totally compatible with the integrated optoelectronic systems. Although it allows for easy fabrication by lithographical processes, this structure cannot be utilized for low-cost flexible photodetectors.⁴⁵

Typical metal-semiconductor-metal (MSM) photodetectors simply produce electrical signals (i.e., current) through the absorption of photons. Photoabsorption results in the generation of **photo-excited electrons** and holes that are drifted under the electric field applied externally between two metal contacts. Planar photodetectors are fast and highly sensitive. Up to date, planar MSM photodetectors with Si NWs were formed through the deposition of metallic contacts on both sides of a single nanowire or multiple nanowires. These structures suffer from the low-photo induced current.⁴⁴ Moreover, the electrical contacts in these devices consist of metallic thin films deposited by vacuum based methods that increase the cost of fabrication and deteriorate the device properties due to the shadowing effect. Some studies have recently been carried out in order to find alternatives such as indium tin oxide (ITO) which is used as a

^{a)}Author to whom correspondence should be addressed. Electronic mail: unalan@metu.edu.tr

transparent top contact in such devices.³⁶ However, vacuum deposition, limited indium sources, and a lack of flexibility are still the inherent problems of using ITO.

Among the alternative transparent and conducting contacts, random networks of silver (Ag) NWs could be a promising candidate. These transparent nanowire electrodes show no shadowing effect on devices and offer flexibility.^{46–48}

Here, we report on the fabrication and characterization of the solution processed Si NW network based MSM photodetectors. Although buckling of Si NWs on elastomeric substrates have been studied^{49,50} and Si NW network based devices have been shown for FET applications,^{51,52} these structures had not been studied for flexible photodetection.

All of the chemicals were purchased from Merck[®] and Sigma[®] Aldrich and used without further purification. For the Si NW fabrication, the MAE method, as reported elsewhere, was followed.¹⁷ The cleaning process was applied to Si wafers (400 μm thick, $\langle 100 \rangle$ orientation, p-type, resistivity 5–10 $\Omega \cdot \text{cm}$) prior to etching. Si wafers were cleaned with consecutive sonication in acetone (99.8%), isopropanol (99.8%), and deionized (DI) water baths for 15 min. To remove metal and organic residues from the wafer, boiling piranha solution was prepared by mixing sulfuric acid (H_2SO_4 , 95%–97%) and hydrogen peroxide (H_2O_2 , 35%) by a volume ratio of 3:1, and the samples were immersed into this solution for 1 h. The samples were dipped into diluted hydrofluoric acid (HF) (38%–40%) solution for the removal of native oxide. A MAE solution was prepared by mixing HF (38%–40%) and AgNO_3 (99.5%) at a molar ratio of 4.6M:0.02M.

In a standard procedure, immersing Si wafer into this solution reduces the dissolved Ag ions to form Ag nanoparticles on Si. The interface between Ag nanoparticles and Si gets anodically oxidized due to the electron transfer between Si and Ag. The silicon dioxide (SiO_2) is dissolved by HF, which allows Ag nanoparticles to sink further into the Si wafer. These reactions are spontaneous and continue unless stopped by removing the sample from the solution. At the end, vertical arrays of Si NWs are formed on Si wafer.

All the etching procedures have been carried out at room temperature with an etching rate of 20 $\mu\text{m}/\text{h}$. Following the achievement of the desired nanowire length, etching was finalized by rinsing samples with DI water. Ag dendrites, which were formed as by-products of MAE, were removed through a nitric acid (DI water 1:3 HNO_3 by vol. ratio) rinse.

Ag NWs were synthesized using the polyol method as reported elsewhere.⁵³ In a typical experiment, 0.45M of polyvinylpyrrolidone (PVP) (MW = 55 000) and 7 mg of sodium chloride (NaCl) (99.5%) were dissolved in 10 ml ethylene glycol (EG) and heated to 170 $^\circ\text{C}$ in a silicon oil bath. In the meantime, a 0.12M AgNO_3 (99.5%) solution in 5 ml of EG was prepared and added drop-wise into the PVP solution by a syringe pump at a rate of 5 ml/h. The solution was stirred at a rate of 1000 rpm by a magnetic stirrer throughout the whole process. Following their synthesis, Ag NWs were purified via multiple centrifuging processes (dispersion in acetone and ethanol, 8000 rpm for 20 min) and then re-dispersed in ethanol. Purified Ag NWs were coated onto glass and polyethylene terephthalate (PET) substrates through spray coating. Following deposition, Ag NW networks were annealed at 200 $^\circ\text{C}$ for

20 min in order to remove residual PVP and thus decrease the junction resistance of NWs at junction points.

For the fabrication of devices, Ag NW networks with a transmittance (at 550 nm) and sheet resistance of 83% and 15 Ω/sq , respectively, was used as electrodes. A 40 μm channel within the Ag NW network formed by mechanical means (i.e., razor blade) served as the channel in photodetectors. Si NW networks were then transferred onto the Ag NW network.

To fabricate Si NW network photodetectors, the native oxide of the Si NWs were removed by a diluted HF (38%–40%) solution (volume ratio 1:20). Afterwards, Si NWs were dispersed in DI water through sonication. Si NW networks were then fabricated through simple vacuum filtration and stamping process. NW density in the network was controlled during vacuum filtration where a desired amount of solution was filtered.

Si NWs and the devices were characterized through a scanning electron microscope (SEM) using FEI[®] Nova Nano SEM 430 microscope operated at 10 kV. Current-voltage (I-V) characteristics of the photodetectors were obtained using a Keithley 2400 sourcemeter, while a AM 1.5G (100 mW/cm^2) solar simulator was used as the light source. Light ON-OFF measurements were conducted at a bias of 5 V. The rise and fall time of the photodetectors were measured with the Agilent[®] brand oscilloscope (10 M Ω oscilloscope probe) using a 1.3 mW Xenon light source (Cermax[®] Xe fiber optic light source) around a 3 mm diameter circle illuminated area and chopped (NewFocus[®] 3501) at 200 Hz under 2.5 V bias. Transmittance measurements were made through the same Xe light source. The spectral photoresponsivity of the photodetector with a 10 V bias was measured using 100 W QTH lamp (Oriel[®] instruments), Cornerstone 260 1/4 m monochromator (Oriel instruments 74100), and Keithley 2440 source meter. The light power was measured using a single channel power meter (Newport[®] 1936-c). All of the measurements were made at atmospheric conditions and room temperature.

Photograph on the left and right hand side of Figure 1(a) shows Si wafer with vertically aligned NW arrays formed by the MAE process and Si NWs dispersed in DI water after sonication. As revealed by the SEM image, the length of Si NWs used in this work was approximately 40 μm . In order to control the density of the Si NWs in the solution, 1 cm^2 area of Si NW containing silicon wafer was immersed in 20 ml of DI Water (18.3 M $\Omega \cdot \text{cm}$) following oxide removal. Only a few seconds of sonication was enough for the rupture of Si NWs from their roots and their consequent dispersion. Further sonication was avoided to prevent NW damage. Si NW dispersion was achieved as evidenced by the brownish color of the solution. The solution was kept at room temperature for a few hours for the precipitation of large NW bundles. Then, the Si NW solution with a known volume was vacuum filtered and a network was formed on a mixed cellulose ester (MCE) membrane as shown in Figure 1(b). Following vacuum filtration, Si NW networks were transferred onto substrates through simple stamping processes. A photograph of a semi-transparent Si NW network deposited onto glass substrate is also shown in Figure 1(b).

The NW density was calculated via the Image J[®] analysis software program using the SEM images shown in

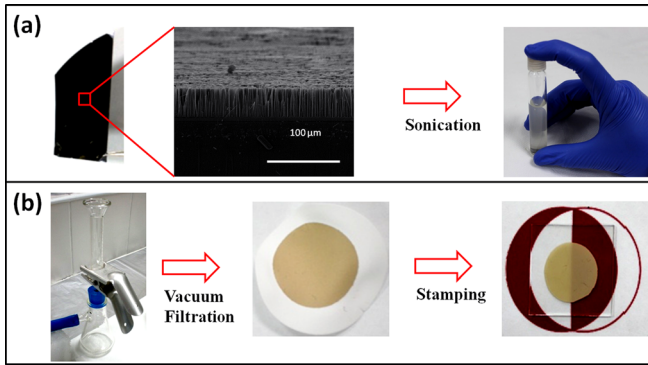


FIG. 1. (a) A photograph of Si wafer with Si NW arrays, SEM image of vertically aligned Si NWs and Si NWs dispersed in water. (b) Photographs of the vacuum filtration setup, Si NW networks on filtration membrane and on glass.

Figures 2(a)–2(c). NW density was determined to be 0.87, 1.87, and 3.44 $\text{NWs}/\mu\text{m}^2$ for the filtered solution volumes of 2.5, 5, and 10 ml, respectively. Variations of the transparency of Si NW networks with different densities are provided in Figure 2(d). For comparison, the transmittance spectrum of the Ag NW network was also provided in the same figure. As expected, the transmittance of the NW networks decrease with increasing NW density.

Figure 3(a) shows a SEM image of Si and Ag NW based MSM photodetectors. The channel was free from Ag NWs following mechanical scratching as shown in the inset of Figure 3(a), which was also assured through electrical measurements. A schematic of the devices fabricated and investigated in this work is provided in Figure 3(b). Following the deposition of the NWs and creating the MSM structure, Ag contact pads were formed by colloidal silver paste for electrical measurements. The active area of the device was 3 mm^2 . A photograph of the finalized device is provided in Figure 3(c).

Figure 4(a) shows the photoresponsivity of the Si NW network photodetectors with different NW densities in the wavelength range of 400 to 1000 nm under a 10 V bias. As

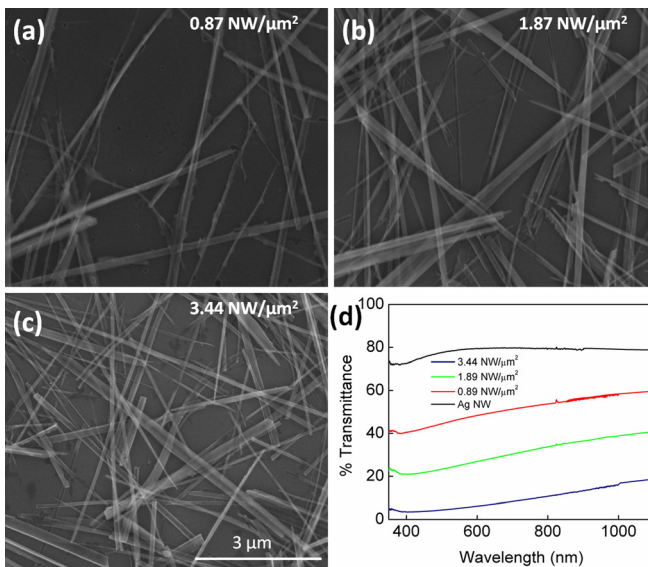


FIG. 2. SEM images of Si NW networks with different densities of (a) 0.87, (b) 1.87, and (c) 3.44 $\text{NWs}/\mu\text{m}^2$. (d) Transparency of Si NW networks with different densities. Transmittance of Ag NW network is also provided for comparison.

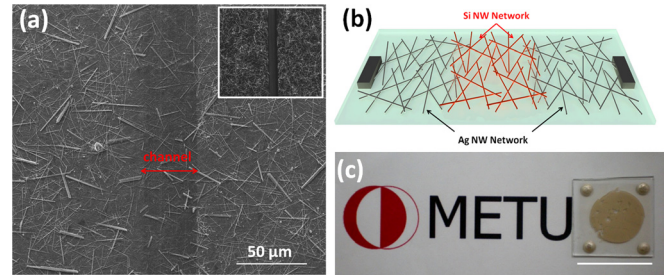


FIG. 3. (a) SEM image of the MSM structure. Inset shows that the channel was free from Ag NW prior to Si NWs transfer. (b) Representative device architecture and (c) photograph of the final device. Scale bar corresponds to 2.5 cm.

expected, NW density was found to increase the responsivity of the fabricated devices. The photoresponse of the devices was found to decrease with increasing wavelength. The decrease in the responsivity could be attributed to lower photon energies and decreased absorption at longer wavelengths (see Figure 2(d)). I–V measurements showed that fabricated MSM photodetectors had a small Schottky barrier at low voltages due to semiconductor NW-NW junctions in the network devices, as shown in Figure 4(b). From the light ON/OFF measurements, photodetectors were found to exhibit fully reversible switching behavior, as shown in Figure 4(c). We also see that both the dark and photo current of the devices increase with NW density. The increase in the dark current is a result of the creation of alternative conduction paths in the random Si NW network. The enhancement in the photo current, on the other hand, is due to enhanced carrier generation from the increased number of NWs in the active medium of the device.

The rise and fall time (dynamic response) of the devices, as shown in Figure 4(d), were measured under a 5 V bias. The rise time of the device was determined by measuring the time necessary for the current to increase from 10% to 90% of its saturation value, whereas the fall time was defined as the time necessary for the current to decrease from 90% to 10% of its saturation value. There was no significant change

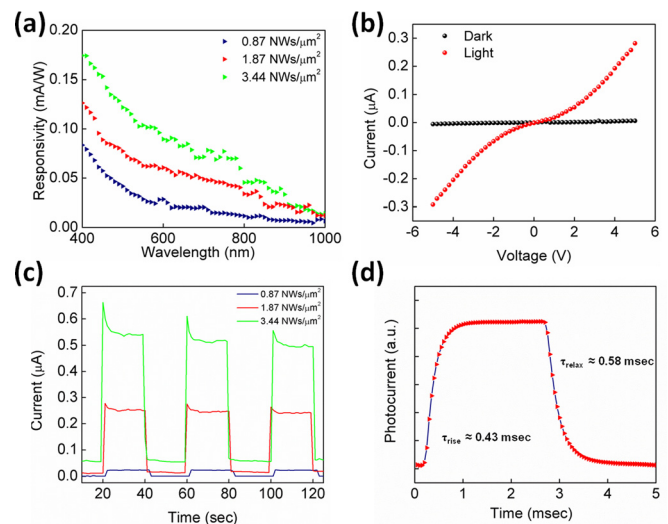


FIG. 4. (a) Photoresponsivity with different NW densities under a 10 V bias. (b) I–V characteristics of the device (1.87 $\text{NWs}/\mu\text{m}^2$). (c) Light ON–OFF measurements with different NW densities under 5 V bias and (d) dynamic response behavior (1.87 $\text{NWs}/\mu\text{m}^2$) under a 5 V bias.

in the dynamic response of the devices with different NW densities or applied bias. This clearly indicates that NW-NW junctions determine trapping/detrapping of the carriers. The typical rise time was found to be 0.43 ms, while the fall time was 0.58 ms. The fall time was relatively high compared with the rise time, which could be related to the deep trap levels created by the defects on the nanowire surface. The surface passivation of the nanowires could be utilized as a solution to improve the photoresponsivity and dynamic response of the devices.

A comparison can be made with Si photodiodes fabricated by Li *et al.*⁵⁴ using high quality float zone Si substrates. The typical rise and fall times of 0.55 and 0.3 ms were obtained in this device, respectively. This signifies that our devices exhibit competitive dynamic response values compared to that of the typical Si photodiodes. On the other hand, photodetectors utilizing Si NW arrays with a vertical structure showed higher responsivity with a faster dynamic response.^{36,44} These superior characteristics were due to the better light trapping, higher carrier generation, and collection efficiencies owing to the vertical NW structure. Moreover, the collection efficiency was enhanced in these vertical structures due to the reduced carrier entrapment at the NW junctions. Since the NW arrays were not detached from the substrate, collection efficiencies were also considerably high. Compared to this vertically aligned system, the NW network photodetectors studied in this work exhibit slightly lower responsivity and slower temporal response. Light trapping is less pronounced for planar NW network devices (as evident from the color of the samples), and therefore, results in poor light absorption and less carrier generation. In addition, the trapping of photogenerated carriers at the adjacent NW-NW junctions deteriorated the charge collection efficiency of the fabricated photodetectors. However, NW networks offer easy and cost-effective fabrication, partial transparency, and flexibility. The combination of these properties within a photodetector structure could only be realized through the use of planar NW networks.

In order to test the flexibility of the MSM photodetectors, the devices ($1.87 \text{ NW}/\mu\text{m}^2$) fabricated on PET substrate underwent a bending test as shown in Figure 5. The photoconductor performance was recorded as a function of number of bending cycles for a fixed bending curvature of 1 cm. Figure 5(a) shows the light ON/OFF measurements upon bending. Devices on glass substrates were treated with dilute HF prior to the measurement while devices on PET substrates were not. The reproducible ON/OFF characteristics were obtained with at least an order of magnitude lower current compared to devices on glass substrates. The I-V characteristics of the device both in the dark and illuminated case are shown in Figure 5(b), showing similar behavior as in the case of devices fabricated on glass substrates. The dark and photo current of the device measured as a function of cycles up to a maximum bending cycles of 500 are shown in Figure 5(c). Bending resulted in a decrease in both the light and dark current of the device during the first 200 cycles; however, further increase in the number of bending cycles did not lead to any change in the current. The decrease in the dark and photo current could be due to the loss of mechanical contacts between Si NW junctions and also Ag and Si

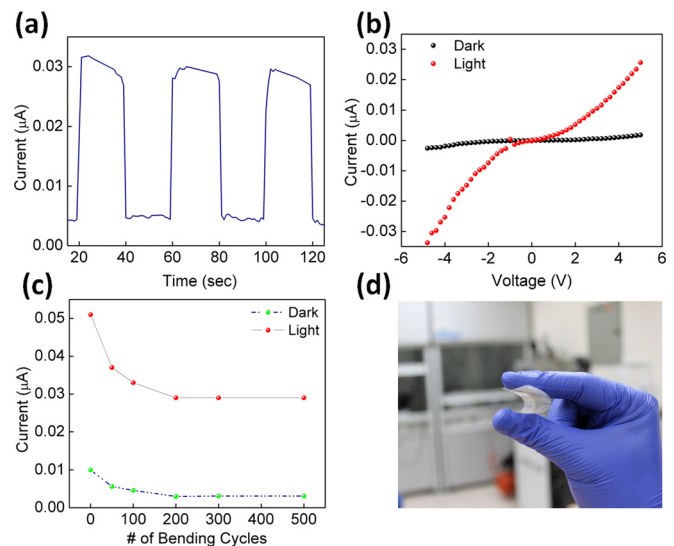


FIG. 5. (a) Light ON-OFF measurements under 5 V bias showing device is operational upon bending. (b) I-V characteristics of the bent device. (c) Dark/light currents under a bias of 5 V showing stability of the devices in the investigated range. (d) Photograph of flexible device at a bending radius of 1 cm. A density of $1.87 \text{ NWs}/\mu\text{m}^2$ was used for flexible devices.

NWs. After 200 cycles, bending did not lead to any further contact loss, and therefore, a stable value was achieved.

In this work, NW network MSM photodetectors have been demonstrated. Fabricated photodetectors showed partial transparency, fully reversible switching behavior (with a switching ratio of ~ 20), and fast dynamic response with a rise and fall time of 0.43 and 0.58 ms, respectively. Almost the same device characteristics were obtained for the devices fabricated on flexible substrates. The results presented herein provide the basis for the fabrication of cost-effective and flexible photodetectors using Si NWs in a network form. The Si NW networks offer flexibility to the Si world and could certainly be used for the fabrication of other optoelectronic and sensing devices.

We would like to thank Yasemin Gizem Fillik for the composition of Figure 3(b). S.C. acknowledges support from METU-OYP Project No. 1439. H.E.U. acknowledges support from the Distinguished Young Scientist Award of the Turkish Academy of Sciences (TUBA). METU Central Laboratory facilities are also greatly acknowledged. The efforts of Bilkent University are supported by the projects DPT-HAMIT, ESF-EPIGRAT, and NATO-SET-181, and TUBITAK under the Project Nos. 107A004, 109A015, and 109E301.

¹J. S. Jie, W. J. Zhang, K. Q. Peng, G. D. Yuan, C. S. Lee, and S. T. Lee, *Adv. Funct. Mater.* **18**(20), 3251–3257 (2008).

²R. S. Wagner and W. C. Ellis, *Appl. Phys. Lett.* **4**(5), 89 (1964).

³C. C. Buttner, N. D. Zakharov, E. Pippel, U. Gosele, and P. Werner, *Semicond. Sci. Technol.* **23**(7), 075040 (2008).

⁴J. D. Holmes, K. P. Johnston, R. C. Doty, and B. A. Korgel, *Science* **287**(5457), 1471–1473 (2000).

⁵A. M. Morales and C. M. Lieber, *Science* **279**(5348), 208–211 (1998).

⁶R. V. Martinez, J. Martinez, and R. Garcia, *Nanotechnology* **21**(24), 245301 (2010).

⁷Y. Q. Fu, A. Colli, A. Fasoli, J. K. Luo, A. J. Flewitt, A. C. Ferrari, and W. I. Milne, *J. Vacuum Sci. Technol. B* **27**(3), 1520–1526 (2009).

⁸X. Li and P. W. Bohn, *Appl. Phys. Lett.* **77**(16), 2572–2574 (2000).

- ⁹T. Qiu, X. L. Wu, G. G. Siu, and P. K. Chu, *J. Electron. Mater.* **35**(10), 1879–1884 (2006).
- ¹⁰S. L. Cheng, C. H. Chung, and H. C. Lee, *J. Electrochem. Soc.* **155**(11), D711–D714 (2008).
- ¹¹C. Y. Chen, C. S. Wu, C. J. Chou, and T. J. Yen, *Adv. Mater.* **20**(20), 3811 (2008).
- ¹²K. Q. Peng, J. J. Hu, Y. J. Yan, Y. Wu, H. Fang, Y. Xu, S. T. Lee, and J. Zhu, *Adv. Funct. Mater.* **16**(3), 387–394 (2006).
- ¹³D. Kumar, S. K. Srivastava, P. K. Singh, K. N. Sood, V. N. Singh, N. Dilawar, and M. Husain, *J. Nanopart. Res.* **12**(6), 2267–2276 (2010).
- ¹⁴K. Q. Peng, Y. J. Yan, S. P. Gao, and J. Zhu, *Adv. Mater.* **14**(16), 1164–1167 (2002).
- ¹⁵K. Q. Peng and J. Zhu, *Electrochim. Acta* **49**(16), 2563–2568 (2004).
- ¹⁶K. Q. Peng, H. Fang, J. J. Hu, Y. Wu, J. Zhu, Y. J. Yan, and S. Lee, *Chem.-Eur. J.* **12**(30), 7942–7947 (2006).
- ¹⁷B. Ozdemir, M. Kulakci, R. Turan, and H. E. Unalan, *Nanotechnology* **22**(15), 155606 (2011).
- ¹⁸K. Q. Peng, Y. Wu, H. Fang, X. Y. Zhong, Y. Xu, and J. Zhu, *Angew. Chem., Int. Ed.* **44**(18), 2737–2742 (2005).
- ¹⁹M. Kulakci, F. Es, B. Ozdemir, H. E. Unalan, and R. Turan, *IEEE J. Photovoltaics* **3** (1), 548–553 (2013).
- ²⁰B. Ozdemir, M. Kulakci, R. Turan, and H. E. Unalan, *Appl. Phys. Lett.* **99**(11), 113510 (2011).
- ²¹B. Z. Tian, X. L. Zheng, T. J. Kempa, Y. Fang, N. F. Yu, G. H. Yu, J. L. Huang, and C. M. Lieber, *Nature* **449**(7164), 885–888 (2007).
- ²²L. Hu and G. Chen, *Nano Lett.* **7**(11), 3249–3252 (2007).
- ²³B. M. Kayes, H. A. Atwater, and N. S. Lewis, *J. Appl. Phys.* **97**(11), 114302 (2005).
- ²⁴E. C. Garnett and P. D. Yang, *J. Am. Chem. Soc.* **130**(29), 9224 (2008).
- ²⁵L. Tsakalacos, J. Balch, J. Fronheiser, B. A. Korevaar, O. Sulima, and J. Rand, *Appl. Phys. Lett.* **91**(23), 233117 (2007).
- ²⁶T. Stelzner, M. Pietsch, G. Andra, F. Falk, E. Ose, and S. Christiansen, *Nanotechnology* **19**(29), 295203 (2008).
- ²⁷K. Q. Peng, Y. Xu, Y. Wu, Y. J. Yan, S. T. Lee, and J. Zhu, *Small* **1**(11), 1062–1067 (2005).
- ²⁸V. Sivakov, G. Andra, A. Gawlik, A. Berger, J. Plentz, F. Falk, and S. H. Christiansen, *Nano Lett.* **9**(4), 1549–1554 (2009).
- ²⁹V. Schmidt, H. Riel, S. Senz, S. Karg, W. Riess, and U. Gosele, *Small* **2**(1), 85–88 (2006).
- ³⁰J. Goldberger, A. I. Hochbaum, R. Fan, and P. D. Yang, *Nano Lett.* **6**(5), 973–977 (2006).
- ³¹A. I. Hochbaum, R. K. Chen, R. D. Delgado, W. J. Liang, E. C. Garnett, M. Najarian, A. Majumdar, and P. D. Yang, *Nature* **451**(7175), 163–165 (2008).
- ³²A. I. Boukai, Y. Bunimovich, J. Tahir-Kheli, J. K. Yu, W. A. Goddard, and J. R. Heath, *Nature* **451**(7175), 168–171 (2008).
- ³³C. K. Chan, R. N. Patel, M. J. O’Connell, B. A. Korgel, and Y. Cui, *ACS Nano* **4**(3), 1443–1450 (2010).
- ³⁴C. K. Chan, H. L. Peng, G. Liu, K. McIlwrath, X. F. Zhang, R. A. Huggins, and Y. Cui, *Nat. Nanotechnol.* **3**(1), 31–35 (2008).
- ³⁵F. Qian, S. Gradecak, Y. Li, C. Y. Wen, and C. M. Lieber, *Nano Lett.* **5**(11), 2287–2291 (2005).
- ³⁶J. Bae, H. Kim, X. M. Zhang, C. H. Dang, Y. Zhang, Y. J. Choi, A. Nurmikko, and Z. L. Wang, *Nanotechnology* **21**(9), 095502 (2010).
- ³⁷S. J. Choi, Y. C. Lee, M. L. Seol, J. H. Ahn, S. Kim, D. I. Moon, J. W. Han, S. Mann, J. W. Yang, and Y. K. Choi, *Adv. Mater.* **23**(34), 3979 (2011).
- ³⁸H. Zhou, G. J. Fang, L. Y. Yuan, C. Wang, X. X. Yang, H. H. Huang, C. H. Zhou, and X. Z. Zhao, *Appl. Phys. Lett.* **94**(1), 013503 (2009).
- ³⁹S. Manna, S. Das, S. P. Mondal, R. Singha, and S. K. Ray, *J. Phys. Chem. C* **116**(12), 7126–7133 (2012).
- ⁴⁰K. H. Kim, K. Keem, D. Y. Jeong, B. D. Min, K. A. Cho, H. Kim, B. Moon, T. Noh, J. Park, M. Suh, and S. Kim, *Jpn. J. Appl. Phys., Part 1* **45**(5A), 4265–4269 (2006).
- ⁴¹P. Servati, A. Colli, S. Hofmann, Y. Q. Fu, P. Beecher, Z. A. K. Durrani, A. C. Ferrari, A. J. Flewitt, J. Robertson, and W. I. Milne, *Physica E* **38**(1–2), 64–66 (2007).
- ⁴²A. Zhang, S. F. You, C. Soci, Y. S. Liu, D. L. Wang, and Y. H. Lo, *Appl. Phys. Lett.* **93**(12), 121110 (2008).
- ⁴³C. Yang, C. J. Barrelet, F. Capasso, and C. M. Lieber, *Nano Letters* **6**(12), 2929–2934 (2006).
- ⁴⁴M. M. Adachi, K. Wang, F. Chen, and K. S. Karim, *Proc. SPIE* **7622**, 76224M (2010).
- ⁴⁵A. Zhang, S. F. You, C. Soci, D. L. Wang, Y. H. Lo, and IEEE, *Planar and Vertical Si Nanowire Photodetectors* (IEEE, New York, 2008).
- ⁴⁶B. Aksoy, S. Coskun, S. Kucukyildiz, and H. E. Unalan, *Nanotechnology* **23**(32), 325202 (2012).
- ⁴⁷S. De, T. M. Higgins, P. E. Lyons, E. M. Doherty, P. N. Nirmalraj, W. J. Blau, J. J. Boland, and J. N. Coleman, *ACS Nano* **3**(7), 1767–1774 (2009).
- ⁴⁸F. Xu and Y. Zhu, *Adv. Mater.* **24**(37), 5117–5122 (2012).
- ⁴⁹S. Y. Ryu, J. L. Xiao, W. Il Park, K. S. Son, Y. Y. Huang, U. Paik, and J. A. Rogers, *Nano Lett.* **9**(9), 3214–3219 (2009).
- ⁵⁰F. Xu, W. Lu, and Y. Zhu, *ACS Nano* **5**(1), 672–678 (2011).
- ⁵¹K. J. Moon, T. I. Lee, J. H. Choi, J. Jeon, Y. H. Kang, J. P. Kar, J. H. Kang, I. Yun, and J. M. Myoung, *ACS Nano* **5**(1), 159–164 (2011).
- ⁵²K. Heo, E. Cho, J. E. Yang, M. H. Kim, M. Lee, B. Y. Lee, S. G. Kwon, M. S. Lee, M. H. Jo, H. J. Choi, T. Hyeon, and S. Hong, *Nano Lett.* **8**(12), 4523–4527 (2008).
- ⁵³S. Coskun, B. Aksoy, and H. E. Unalan, *Cryst. Growth Des.* **11**(11), 4963–4969 (2011).
- ⁵⁴X. Li, J. E. Carey, J. W. Sickler, M. U. Pralle, C. Palsule, and C. J. Vineis, *Opt. Express* **20**(5), 5518–5523 (2012).